Trans. Japan Soc. Aero. Space Sci.
Vol. 48, No. 160, pp. 102–109, 2005

Optimal Flow Control Using Unsteady Sensitivity Analysis

By Hyoung-Jin KIM,[1)] Chongam KIM[2)] and Oh-Hyun RHO[2)]

[1)]*Department of Aerospace Engineering, Tohoku University, Sendai, Japan*
[2)]*Department of Aerospace Engineering, Seoul National University, Seoul, Korea*

(Received November 15th, 2004)

This paper describes an optimal flow control method for compressible laminar/turbulent flows utilizing discrete unsteady aerodynamic sensitivity analysis methods. Unsteady aerodynamic sensitivity codes are developed using a direct differentiation method and an adjoint method, respectively, from two-dimensional unsteady compressible Navier-Stokes equations. Optimal flow controls are conducted by minimizing an unsteady objective function defined at an instant instead of integrating a response for a period of time. Unsteady sensitivity derivatives of the objective function are calculated by the unsteady sensitivity codes, and optimization is conducted utilizing a linear line search method at every physical time step. Several flow control examples of academic interest including circular cylinder vortex shedding control and airfoil shock buffet control show satisfactory results. The present active flow control method utilizing the unsteady sensitivity analysis is robust and problem independent compared to conventional active control methods.

Key Words: Flow Control, Unsteady Sensitivity Analysis, Adjoint Method

1. Introduction

Flow control has been one of the major research topics in aerodynamics and hydrodynamics, since it has much potential ability to improve the performance and efficiency of various fluid dynamic configurations. With the recent development of computational fluid dynamics, optimal flow control methods utilizing Navier-Stokes equations and sensitivity analysis methods are gaining much more attention than before. Optimal flow control methods make it possible to conduct feedback flow control without any a priori knowledge of the unsteady flow characteristics.

Optimal flow control methods have been mainly developed for incompressible low Reynolds number flows since the flow equations are much simpler than compressible flows. Joslin et al.[1)] applied a coupled system of unsteady incompressible Navier-Stokes equations, an adjoint Navier-Stokes system and optimality conditions to the problem of boundary layer instability suppression. Temam et al.[2)] applied an optimal feedback control method utilizing an adjoint method to a low-Reynolds-number turbulent channel flow to obtain a significant reduction in drag force. Min and Choi[3)] employed a suboptimal feedback control method for the vortex shedding control of a circular cylinder wake flow. Here 'suboptimal' means, 'the objective function at an instant is sequentially minimized instead of an integrated one over a period of time'.

Although there has been much literature on the optimal flow control for incompressible low Reynolds number flows, few studies have been done on compressible high Reynolds number flows. Mohammadi[4)] reported a flow control method for high-speed flows using incomplete sensitivity derivatives. He assumed that the sensitivity derivatives with respect to flow variables can be neglected if the objective function is based on local information around the body surface. This method, however, would have trouble being applied to flow control problems such as those with blowing/suction or with an objective function other than body surface integration. Therefore, a general flow control method using complete sensitivity information is required.

The objective of the present study is to develop a general active flow control method utilizing an unsteady complete sensitivity analysis method for compressible laminar or turbulent flows. Unsteady sensitivity analysis codes are developed for discrete unsteady Navier-Stokes equations with the Baldwin-Lomax algebraic turbulence model from steady sensitivity codes developed in previous research by the authors.[5)] The objective function is minimized at each physical time level determining flow control inputs by a simple line search method, which can be easily replaced with more sophisticated gradient-based algorithms at the cost of computational time.

We also present a brief explanation of the flow solver used in this study, and the formulations for unsteady sensitivity analysis for both of sequential and integrated objective functions are given using a discrete approach. Flow control examples are then conducted including circular cylinder vortex shedding control and supercritical airfoil buffet control problems. Finally, a conclusion is made.

2. Flow Analysis

A two-dimensional unsteady Navier-Stokes solver developed and validated in previous studies[6,7)] was used for the flow analysis. Unsteady Reynolds-averaged two-dimensional compressible Navier-Stokes equations in generalized coordinates are used in the conservation form based on a cell-centered finite volume approach, given as

$$\frac{1}{J}\frac{\partial \boldsymbol{Q}}{\partial t} + \boldsymbol{R} = 0, \tag{1}$$

where J is the Jacobian for the grid, t is physical time, $\boldsymbol{Q}$ is a four-element vector of conserved flow variables as $\boldsymbol{Q} = \{\rho, \rho u, \rho v, \rho e\}^{\mathrm{T}}$, and $\boldsymbol{R}$ is the residual vector as $\boldsymbol{R} = (\boldsymbol{E} - \boldsymbol{E}_{\mathrm{v}})_{\xi} + (\boldsymbol{F} - \boldsymbol{F}_{\mathrm{v}})_{\eta}$. $\boldsymbol{E}$ and $\boldsymbol{F}$ are inviscid flux vectors and $\boldsymbol{E}_{\mathrm{v}}$ and $\boldsymbol{F}_{\mathrm{v}}$ are viscous vectord in generalized coordinates, respectively.

Roe's Flux Difference Splitting (FDS) scheme was adopted for the space discretization in the inviscid flux terms of the residual vector on the right-hand side; the MUSCL approach with the Koren limiter is employed to obtain third-order accuracy. The central difference method is used for viscous flux terms of the residual vector. Turbulence effects were considered using the Baldwin-Lomax algebraic model with a relaxation technique. All boundary conditions were specified explicitly. One-dimensional characteristic conditions were used for the inflow and outflow boundaries. The no-slip condition and adiabatic wall condition were specified on the solid wall.

For temperal discretization, the dual-time stepping method is employed to obtain second-order temperal accuracy as follows:

$$\frac{1}{J}\frac{\partial \boldsymbol{Q}}{\partial \tau} = -\boldsymbol{R}^{n+1,s} - \frac{3\boldsymbol{Q}^{n+1,s} - 4\boldsymbol{Q}^{n} + \boldsymbol{Q}^{n-1}}{2J\Delta t}, \tag{2}$$

where τ represents the pseudo time, n is the physical time level, and s is the pseudo time level. The above equations are discretized in pseudo time using the Euler implicit method and linearized by employing the flux Jacobian. This results in a large system of linear equations in delta form at each pseudo time step as:

$$\left(\frac{I}{J\Delta\tau} + \frac{\partial \boldsymbol{R}}{\partial \boldsymbol{Q}} + \frac{1.5I}{J\Delta t}\right)\Delta \boldsymbol{Q} = -\boldsymbol{R}^{n+1,s} - \frac{3\boldsymbol{Q}^{n+1,s} - 4\boldsymbol{Q}^{n} + \boldsymbol{Q}^{n-1}}{2J\Delta t}, \tag{3}$$

where I is an identity matrix.

In the implicit part, Beam & Warming's Alternating Direction Implicit (ADI) method is used, and van Leer's Flux Vector Splitting (FVS) is employed with first-order accuracy for the flux Jacobian. The flux Jacobian for the viscous part is neglected in the implicit part since it does not influence the solution accuracy. Details of the flow solver can be found in previous resports.[6,7]

3. Unsteady Sensitivity Analysis

For the application of unsteady sensitivity analysis for unsteady flow design and control problems, one may define an objective function as an integral of the instantaneous unsteady objective function for its period T such as $\bar{F} = \int_0^T F(t)\mathrm{d}t$. For inherently periodic flows such as flapping wings, helicopter rotors in forward flight, turbomachinery blades, etc., the integrated objective function appears to be a proper choice.

However, this integrated objective function requires prohibitively large computational time since a flow solver and a sensitivity code should be iteratively analyzed for a period or time. If the number of control parameters is D and the time peroid from 0 to T is discretized by N time levels, direct differentiation methods have $D \times N$ control parameters for which the sensitivity gradient of the objective function should be calculated. In cases of the adjoint method, all of the flow variable data of the time period should be saved in memory. The time-integrated objective function approach seemed to be impractical until now.

An alternative objective function is a suboptimal approach in which the objective function at an instant is sequentially minimized instead of an integrated one over a period of time. This suboptimal approach is very efficient in computational cost compared with the approach with integrated objective functions. However, it may cause misleading results since a former control may cause unfavorable effects later.

In this study, we present formulations of unsteady sensitivity analysis for both integrated and instantaneous objective functions, and the sequential approach is employed for flow control examples.

3.1. Formulation for suboptimal objective function

In the suboptimal approach, an objective function at an instant is sequentially minimized instead of an integrated one over a period of time. The instantaneous objective function F^{n+1} is a function of flow variables $\boldsymbol{Q}$, grid position $\boldsymbol{X}$, and design variables $\boldsymbol{\beta}$ at the $(n+1)$th time level; i.e.,

$$F^{n+1} = F^{n+1}(Q^{n+1}(\beta),\ X^{n+1}(\beta),\ \beta^{n+1}). \tag{4}$$

3.1.1. Direct differentiation method

The sensitivity derivative of the cost function F with respect to design variable vector $\boldsymbol{\beta}$ is given by chain rule as:

$$\frac{\mathrm{d}F^{n+1}}{\mathrm{d}\boldsymbol{\beta}} = \frac{\partial F}{\partial \boldsymbol{Q}}^{\mathrm{T}}\frac{\mathrm{d}\boldsymbol{Q}^{n+1}}{\mathrm{d}\boldsymbol{\beta}} + \frac{\partial F}{\partial \boldsymbol{X}}^{\mathrm{T}}\frac{\mathrm{d}\boldsymbol{X}^{n+1}}{\mathrm{d}\boldsymbol{\beta}} + \frac{\partial F^{n+1}}{\partial \boldsymbol{\beta}}. \tag{5}$$

The discrete residual vector of nonlinear aerodynamic analysis for unsteady problems at the $(n+1)$th physical time level can be written symbolically as:

$$\boldsymbol{R}^{n+1}(\boldsymbol{Q}, \boldsymbol{X}, \boldsymbol{\beta}) + \frac{3\boldsymbol{Q}^{n+1} - 4\boldsymbol{Q}^{n} + \boldsymbol{Q}^{n-1}}{2J\Delta t} = 0, \tag{6}$$

where $\boldsymbol{X}$ is the grid position vector, and $\boldsymbol{\beta}$ is the vector of design variables.

Equation (6) is directly differentiated with respect to $\boldsymbol{\beta}^{n+1}$ to yield the following equation:

$$\left(\frac{\partial \boldsymbol{R}}{\partial \boldsymbol{Q}} + \frac{3}{2J\Delta t}\right)\frac{\mathrm{d}\boldsymbol{Q}^{n+1}}{\mathrm{d}\boldsymbol{\beta}} + \frac{\partial \boldsymbol{R}}{\partial \boldsymbol{X}}\frac{\mathrm{d}\boldsymbol{X}^{n+1}}{\mathrm{d}\boldsymbol{\beta}} + \frac{\partial \boldsymbol{R}^{n+1}}{\partial \boldsymbol{\beta}} = 0 \tag{7}$$

Note that among the flow variable vectors $\boldsymbol{Q}^{n+1}$, $\boldsymbol{Q}^{n}$ and $\boldsymbol{Q}^{n-1}$, only $\boldsymbol{Q}^{n+1}$ is a function of $\boldsymbol{\beta}^{n+1}$.

In order to find the solution $(\mathrm{d}\boldsymbol{Q}/\mathrm{d}\boldsymbol{\beta})^{n+1}$ of the unsteady sensitivity Eq. (7), a pseudo time term is added and the same time integration scheme with the flow solver is adopted to obtain the following form:

$$\left(\frac{I}{J\Delta\tau}+\frac{\partial \boldsymbol{R}}{\partial \boldsymbol{Q}}+\frac{3I}{2J\Delta t}\right)\Delta\left(\frac{\mathrm{d}\boldsymbol{Q}}{\mathrm{d}\boldsymbol{\beta}}\right) = -\left(\left(\frac{\partial \boldsymbol{R}}{\partial \boldsymbol{Q}}+\frac{3I}{2J\Delta t}\right)\frac{\mathrm{d}\boldsymbol{Q}^{n+1,s}}{\mathrm{d}\boldsymbol{\beta}}+\frac{\partial \boldsymbol{R}}{\partial \boldsymbol{X}}\frac{\mathrm{d}\boldsymbol{X}^{n+1}}{\mathrm{d}\boldsymbol{\beta}}+\frac{\partial \boldsymbol{R}^{n+1}}{\partial \boldsymbol{\beta}}\right), \tag{8}$$

where s is the pseudo time level. The flux Jacobian in the left-hand side of Eq. (8) is van Leer's FVS flux Jacobian as the flow analysis. The above system of equations is solved with the same time integration scheme and CFL number with the flow solver.

When the flow variable sensitivity vector $(\mathrm{d}\boldsymbol{Q}/\mathrm{d}\boldsymbol{\beta})^{n+1}$ is obtained, the total derivative of the unsteady system response of interest F^{n+1} can be calculated by Eq. (5).

3.1.2. Adjoint variable method

Since the total derivative of the residual vector of the unsteady flow equations is null in the $(n+1)$th time level as can be seen in Eq. (7), we introduce adjoint variables and combine Eqs. (5) and (7) to obtain

$$\frac{\mathrm{d}F}{\mathrm{d}\boldsymbol{\beta}} = \frac{\partial F}{\partial \boldsymbol{Q}}\frac{\mathrm{d}\boldsymbol{Q}}{\mathrm{d}\boldsymbol{\beta}}+\frac{\partial F}{\partial \boldsymbol{X}}\frac{\mathrm{d}\boldsymbol{X}}{\mathrm{d}\boldsymbol{\beta}}+\frac{\partial F}{\partial \boldsymbol{\beta}} + \boldsymbol{\Lambda}^{\mathrm{T}}\left(\left(\frac{\partial \boldsymbol{R}}{\partial \boldsymbol{Q}}+\frac{1.5}{J\Delta t}\right)\frac{\mathrm{d}\boldsymbol{Q}}{\mathrm{d}\boldsymbol{\beta}} + \frac{\partial \boldsymbol{R}}{\partial \boldsymbol{X}}\frac{\mathrm{d}\boldsymbol{X}}{\mathrm{d}\boldsymbol{\beta}}+\frac{\partial \boldsymbol{R}}{\partial \boldsymbol{\beta}}\right), \tag{9}$$

where superscipt $n+1$ for the physical time level is omitted for simplicity.

Coefficients of flow variable sensitivity vector $\mathrm{d}\boldsymbol{Q}/\mathrm{d}\boldsymbol{\beta}$ form the following adjoint equation:

$$\left(\frac{\partial \boldsymbol{R}}{\partial \boldsymbol{Q}}^{\mathrm{T}}+\frac{1.5I}{J\Delta t}\right)\boldsymbol{\Lambda}+\frac{\partial F}{\partial \boldsymbol{Q}}^{\mathrm{T}}=0 \tag{10}$$

If we find an adjoint variable vector $\boldsymbol{\Lambda}$ that satisfies the above adjoint equation, we can obtain the sensitivity derivative of F with respect to $\boldsymbol{\beta}$ by the following equation without any information about the flow variable sensitivity vector $\mathrm{d}\boldsymbol{Q}/\mathrm{d}\boldsymbol{\beta}$. This makes the computational cost for sensitivity analysis independent of the number of design variables:

$$\frac{\mathrm{d}F}{\mathrm{d}\boldsymbol{\beta}} = \frac{\partial F}{\partial \boldsymbol{X}}\frac{\mathrm{d}\boldsymbol{X}}{\mathrm{d}\boldsymbol{\beta}}+\frac{\partial F}{\partial \boldsymbol{\beta}}+\boldsymbol{\Lambda}^{\mathrm{T}}\left(\frac{\partial \boldsymbol{R}}{\partial \boldsymbol{X}}\frac{\mathrm{d}\boldsymbol{X}}{\mathrm{d}\boldsymbol{\beta}}+\frac{\partial \boldsymbol{R}}{\partial \boldsymbol{\beta}}\right) \tag{11}$$

Adjoint Eq. (10) is also converted to the following system of linear algebraic equations and is solved by the ADI scheme for pseudo time steps with the same CFL number:

$$\left(\frac{I}{J\Delta\tau}+\frac{\partial \boldsymbol{R}}{\partial \boldsymbol{Q}}^{\mathrm{T}}+\frac{1.5I}{J\Delta t}\right)\Delta\boldsymbol{\Lambda} = -\left(\left(\frac{\partial \boldsymbol{R}}{\partial \boldsymbol{Q}}^{\mathrm{T}}+\frac{1.5I}{J\Delta t}\right)\boldsymbol{\Lambda}+\frac{\partial F}{\partial \boldsymbol{Q}}^{\mathrm{T}}\right) \tag{12}$$

The transposed flux Jacobian in the left-hand side of Eq. (12) is van Leer's FVS flux Jacobian as the flow analysis.

3.2. Formulation for integrated objective function

For the periodic flow with a period T, the integrated objective function can be defined as follows:

$$\bar{F} = \int_0^T F(t)\mathrm{d}t \cong \sum_{n=1}^{N} F^n(Q^n, X^n)\Delta t, \tag{13}$$

where we assume that the physical time step Δt is constant in the unsteady computations.

3.2.1. Direct differentiation method

The sensitivity derivative of the integrated objective function with respect to design variable vector $\boldsymbol{\beta}^i$ at an arbitrary time level i is given as follows:

$$\frac{\mathrm{d}\bar{F}}{\mathrm{d}\boldsymbol{\beta}^i} = \sum_{n=0}^{N}\left(\frac{\partial F}{\partial \boldsymbol{Q}}\bigg|_n\frac{\mathrm{d}\boldsymbol{Q}^n}{\mathrm{d}\boldsymbol{\beta}^i}+\frac{\partial F}{\partial \boldsymbol{X}}\bigg|_n\frac{\mathrm{d}\boldsymbol{X}^n}{\mathrm{d}\boldsymbol{\beta}^i}+\frac{\partial F^n}{\partial \boldsymbol{\beta}^i}\right)\Delta t \tag{14}$$

In order to calculate $\mathrm{d}\boldsymbol{Q}^n/\mathrm{d}\boldsymbol{\beta}^i$, one needs to differentiate the discrete residual vector of Eq. (6) with respect to $\boldsymbol{\beta}^i$ to obtain the following direct sensitivity equation:

$$\left(\frac{\partial \boldsymbol{R}}{\partial \boldsymbol{Q}}\bigg|_{n+1}+\frac{3I}{2J_{n+1}\Delta t}\right)\frac{\mathrm{d}\boldsymbol{Q}^{n+1}}{\mathrm{d}\boldsymbol{\beta}^i}-\frac{2I}{J_{n+1}\Delta t}\frac{\mathrm{d}\boldsymbol{Q}^n}{\mathrm{d}\boldsymbol{\beta}^i} + \frac{I}{2J_{n+1}\Delta t}\frac{\mathrm{d}\boldsymbol{Q}^{n-1}}{\mathrm{d}\boldsymbol{\beta}^i}+\frac{\partial \boldsymbol{R}}{\partial \boldsymbol{X}}\bigg|_{n+1}\frac{\mathrm{d}\boldsymbol{X}^{n+1}}{\mathrm{d}\boldsymbol{\beta}^i}+\frac{\partial \boldsymbol{R}^{n+1}}{\partial \boldsymbol{\beta}^i}=0 \tag{15}$$

Note the difference between Eq. (7) for instantaneous objective function and Eq. (15) for the integrated objective function. Equation (15) can also be solved for $\mathrm{d}\boldsymbol{Q}^{n+1}/\mathrm{d}\boldsymbol{\beta}^i$ by adding a pseudo time term as done in Eq. (8).

3.2.2. Adjoint variable method

In order not to calculate the flow variable sensitivity $\mathrm{d}\boldsymbol{Q}/\mathrm{d}\boldsymbol{\beta}$ for the sensitivity analysis, we combine Eq. (14) and Eq. (15) again by introducing an adjoint vector:

$$\frac{\mathrm{d}\bar{F}}{\mathrm{d}\boldsymbol{\beta}^i} = \sum_{n=0}^{N}\Bigg[\frac{\partial F}{\partial \boldsymbol{Q}}\bigg|_n\frac{\mathrm{d}\boldsymbol{Q}^n}{\mathrm{d}\boldsymbol{\beta}^i}+\frac{\partial F}{\partial \boldsymbol{X}}\bigg|_n\frac{\mathrm{d}\boldsymbol{X}^n}{\mathrm{d}\boldsymbol{\beta}^i} + \frac{\partial \boldsymbol{F}^n}{\partial \boldsymbol{\beta}^i}+\Lambda^n\left\{\left(\frac{\partial \boldsymbol{R}}{\partial \boldsymbol{Q}}\bigg|_n+\frac{3I}{2J_n\Delta t}\right)\frac{\mathrm{d}\boldsymbol{Q}^n}{\mathrm{d}\boldsymbol{\beta}^i} - \frac{2I}{J_n\Delta t}\frac{\mathrm{d}\boldsymbol{Q}^{n-1}}{\mathrm{d}\boldsymbol{\beta}^i}+\frac{I}{2J_n\Delta t}\frac{\mathrm{d}\boldsymbol{Q}^{n-2}}{\mathrm{d}\boldsymbol{\beta}^i} + \frac{\partial \boldsymbol{R}}{\partial \boldsymbol{X}}\bigg|_n\frac{\mathrm{d}\boldsymbol{X}^n}{\mathrm{d}\boldsymbol{\beta}^i}+\frac{\partial \boldsymbol{R}^n}{\partial \boldsymbol{\beta}^i}\right\}\Bigg]\Delta t \tag{16}$$

Note that the time index of the direct differentiation equation is reduced by one to match the index with that of the objective function.

We select terms related with $\mathrm{d}\boldsymbol{Q}/\mathrm{d}\boldsymbol{\beta}$ as follows:

$$\sum_{n=0}^{N}\Bigg[\left\{\left(\frac{\partial \boldsymbol{R}}{\partial \boldsymbol{Q}}\bigg|_n+\frac{3I}{2J_n\Delta t}\right)\boldsymbol{\Lambda}^n+\frac{\partial F}{\partial \boldsymbol{Q}}\bigg|_n\right\}\frac{\mathrm{d}\boldsymbol{Q}^n}{\mathrm{d}\boldsymbol{\beta}^i} - \frac{2I}{J_n\Delta t}\boldsymbol{\Lambda}^n\frac{\mathrm{d}\boldsymbol{Q}^{n-1}}{\mathrm{d}\boldsymbol{\beta}^i}+\frac{I}{2J_n\Delta t}\boldsymbol{\Lambda}^n\frac{\mathrm{d}\boldsymbol{Q}^{n-2}}{\mathrm{d}\boldsymbol{\beta}^i}\Bigg]\Delta t = 0 \tag{17}$$

Arranging the above equation for terms with $\mathrm{d}\boldsymbol{Q}/\mathrm{d}\boldsymbol{\beta}$ and setting the coefficent of each $\mathrm{d}\boldsymbol{Q}/\mathrm{d}\boldsymbol{\beta}$ term as zero, we obtain the following adjoint equation for the integrated objective function:

$$\left(\frac{\partial \boldsymbol{R}}{\partial \boldsymbol{Q}}\bigg|_n + \frac{3}{2J_n\Delta t}\right)\boldsymbol{\Lambda}^n - \frac{2I}{J_{n+1}\Delta t}\boldsymbol{\Lambda}^{n+1} + \frac{I}{2J_{n+2}\Delta t}\boldsymbol{\Lambda}^{n+2} + \frac{\partial F}{\partial \boldsymbol{Q}}^{\mathrm{T}}\bigg|_n = 0 \tag{18}$$

The adjoint equation of Eq. (18) is marched in reverse time. Initial conditions are obtained by the following equations at time levels N and $N-1$, which are also obtained from Eq. (18):

$$\left(\frac{\partial \boldsymbol{R}}{\partial \boldsymbol{Q}}\bigg|_N + \frac{3I}{2J_N\Delta t}\right)\boldsymbol{\Lambda}^N + \frac{\partial F}{\partial \boldsymbol{Q}}^{\mathrm{T}}\bigg|_N = 0 \tag{19a}$$

$$\left(\frac{\partial \boldsymbol{R}}{\partial \boldsymbol{Q}}\bigg|_{N-1} + \frac{3I}{2J_{N-1}\Delta t}\right)\boldsymbol{\Lambda}^{N-1} - \frac{2I}{J_N\Delta t}\boldsymbol{\Lambda}^N + \frac{\partial F}{\partial \boldsymbol{Q}}^{\mathrm{T}}\bigg|_{N-1} = 0 \tag{19b}$$

Firstly, the initial adjoint vector $\boldsymbol{\Lambda}_N$ is calculated by Eq. (19a), and $\boldsymbol{\Lambda}_{N-1}$ is calculated using $\boldsymbol{\Lambda}_N$ and Eq. (19b). After that, Eq. (18) can be used for the adjoint vector at the next time level in reverse time.

When the adjoint vectors are calculated, the objective function gradient can be calculated by the following equation:

$$\frac{\mathrm{d}\bar{F}}{\mathrm{d}\boldsymbol{\beta}^i} = \sum_{n=0}^{N}\left[\frac{\partial F}{\partial \boldsymbol{X}}\bigg|_n \frac{\mathrm{d}\boldsymbol{X}^n}{\mathrm{d}\boldsymbol{\beta}^i} + \frac{\partial F^n}{\partial \boldsymbol{\beta}^i} + \boldsymbol{\Lambda}^n\left\{\frac{\partial \boldsymbol{R}}{\partial \boldsymbol{X}}\bigg|_n \frac{\mathrm{d}\boldsymbol{X}^n}{\mathrm{d}\boldsymbol{\beta}^i} + \frac{\partial \boldsymbol{R}^n}{\partial \boldsymbol{\beta}^i}\right\}\right]\Delta t \tag{20}$$

As aforementioned, the integrated objective function requires much computational time for the direct method because the number of design parameters is proportional to the number of physical time steps for a period. Also, the adjoint method requires much memory storage because of the reverse time of the adjoint equation. Recently, Nadarajah and Jameson[8] applied the integrated objective function for unsteady design problems of pitching airfoils using two-dimensional Euler equations.

In this study, we employ the suboptimal instantaneous objective functions as the design objective instead of the integrated objective function for flow control examples of physically periodic flows.

4. Flow Control Method

We employed the following two procedures to minimize unsteady objective function F.

Strategy I

(1) Calculate F^{n+1} by flow analysis for $\boldsymbol{\beta}$ at previous physical time level ($\boldsymbol{\beta}^n$)
(2) Calculate ∇F^{n+1} by sensitivity analysis for $\boldsymbol{\beta} = \boldsymbol{\beta}^n$
(3) Calculate $\boldsymbol{\beta}^{n+1}$ as follows.
$$\Delta\boldsymbol{\beta} = -\frac{F}{|\nabla F|^2}\nabla F, \quad \boldsymbol{\beta}^{n+1} = \boldsymbol{\beta}^n + \Delta\boldsymbol{\beta}$$
(4) $n = n+1$, and go to Step 1.

Strategy II

The following step is added to the Strategy I after Step 3.
(3-1) Calculate F^{n+1} again by flow analysis for $\boldsymbol{\beta} = \boldsymbol{\beta}^{n+1}$

Strategy I requires one flow analysis and one sensitivity analysis for a physical time level. There is a time lag between the objective function F and the control parameter $\boldsymbol{\beta}$ because $\boldsymbol{\beta}^n$ is used for the calculation of F^{n+1}. On the other hand, Strategy II requires two flow analyses and one sensitivity analysis for a physical time level. And there is no time lag between the objective function and the control parameter $\boldsymbol{\beta}$ because F^{n+1} is updated for $\boldsymbol{\beta}^{n+1}$ in Step (3-1). Thus, Strategy II is expected to give better results than Strategy I. However, if control parameter variation is not so large in one physical time step, Strategy I may give similar control effects as Strategy II for less computational cost.

In this study, it is assumed that F shows linear bevavior with respect to $\boldsymbol{\beta}$. If the assumption is not valid or does not give satisfactory results, we can apply another line search method such as quadratic line search or a more sophisticated multidimensional optimzation algorithm at the cost of increased computation time.

5. Results and Discussion

In this section, we apply the unsteady sensitivity codes via direct and adjoint methods to flow control examples.

5.1. Cylinder lift control

The first example is a cylinder lift control case, in which we attempt to remove the lift of a cylinder with vortex shedding by adjusting the rotational speed of the cylinder. Flow conditions are $M_\infty = 0.3$, $Re = 200$, in which an asymmetric von Karman vortex is generated and convected in the wake region.

First, we validate the sensitivity codes developed in the previous sections. In order to validate the direct and adjoint unsteady sensitivity codes, unsteady sensitivity derivatives are compared with those calculated by the following finite difference approximation.

$$\frac{\mathrm{d}C_l}{\mathrm{d}\phi}^{n+1} \cong \frac{C_{l,\phi+\Delta\phi}^{n+1} - C_{l,\phi}^{n+1}}{\Delta\phi}, \tag{21}$$

where ϕ is a nondimensional rotating speed defined as $\phi = \omega r/U_\infty$, and r is a cylinder radius. For sensitivity code validation, the residual of the unsteady flow solver is reduced by six orders from a freestream value, and the step size $\Delta\phi$ for the finite difference calculation is 10^{-4}. The residuals of the sensitivity codes are reduced by four orders from their initial residuals.

The initial condition of the sensitivity derivatives $\mathrm{d}\boldsymbol{Q}/\mathrm{d}\phi$ is set by differentiating the initial conditions of the flow solver, and the initial value of adjoint variables $\boldsymbol{\Lambda}$ is set to zero. The physical time step Δt is set to be 0.2 and a CFL number of 5 was used for all computations in this study.

Figure 1 shows the time history of the sensitivity derivative of a lift coefficient C_l' ($=\mathrm{d}C_l/\mathrm{d}\phi$). The sensitivity derivatives by the finite difference and direct and adjoint methods almost coincide exactly with one another. This implies that

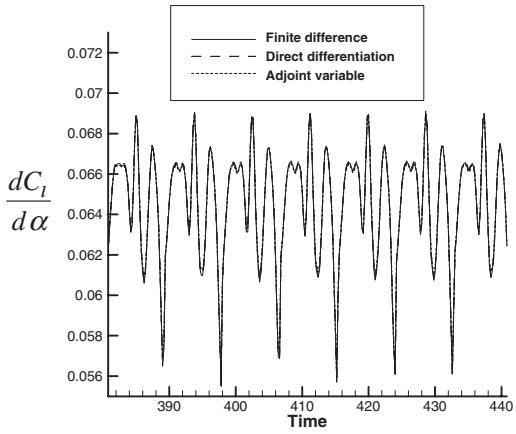

Fig. 1. Validation of unsteady sensitivity analysis codes (Circular cylinder, $Re = 200$, $M_\infty = 0.3$).

the steady sensitivity codes developed in a previous study[5] are successfully converted to unsteady codes.

An objective function is defined as follows to remove the lift of the cylinder:

$$\text{Minimize} \quad F = \frac{1}{2} C_l{}^2 \tag{22}$$

In this case, we used both Strategies I and II for the flow control. For the sensitivity analysis, we adopted the direct sensitivity code since only one control parameter, the rotating speed ϕ, is used in this case, and the adjoint code requires about twice the computation time required by the direct code.[5] In the flow control procedure, the flow solver residual is reduced by five orders from the freestream value. For convergence at each physical time level, about 30–50 pseudo time steps are required. For the sensitivity analysis codes, residual reduction by three orders was enough to obtain accurate unsteady sensitivity derivatives. This requires about two-thirds of the pseudo iteration numbers of the flow analysis.

Figure 2(a) shows lift histories before and after the flow control, and Fig. 2(b) shows variation of rotating speed α to reduce the lift force. The lift and rotating speed α controlled by Strategy I oscillate, while the lift controlled by Strategy II is successfully removed and α does not oscillate. This implies that the simple linear assumption adopted for the calculation of the control parameter variation worked well in this case. Another fact to be noted is that the time lag of Strategy I causes the oscillation of the objective and the control parameter. Therefore, we used only Strategy II for the remaining examples.

5.2. Cylinder vortex shedding control

In this example, the present flow control method is applied to the vortex shedding control problem of a circular cylinder. We defined the objective function as the squared difference between the target surface pressures and the computed surface pressures of the cylinder, as follows.

$$\text{Minimize} \quad F = \frac{1}{2} \int_0^{2\pi} (C_\mathrm{p} - C_\mathrm{pt})^2 R \mathrm{d}\theta. \tag{23}$$

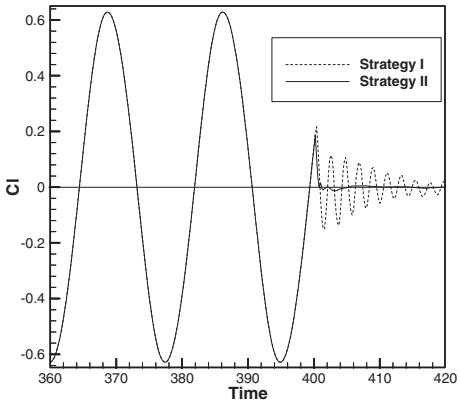

(a) Time history of lift coefficient (flow control was started at $t = 400.4$).

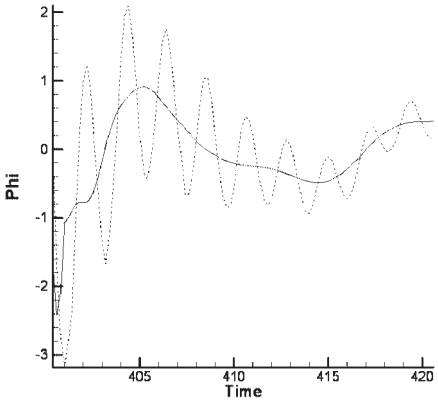

(b) Variation of control parameter α.

Fig. 2. Cylinder lift control results ($Re = 200$, $M_\infty = 0.3$).

The target pressures C_pt are specified as those of the inviscid flow given as $1 - 4\sin^2\theta$ where θ is the circumferential coordinate of the polar coordinate system. The above objective function was reported in a previous study[3] to give better vortex shedding control performance than other objectives tested such as pressure drag or pressure gradient minimization on the cylinder surface.

We employed blowing/suction velocities along the cylinder surface as control parameters with a constraint that the blowing/suction velocities should be less than 40% of the freestream Mach number. Since there are a large number of control parameters, the adjoint sensitivity code is used here.

Figure 3(a) shows the time history of the objective function F before and after the control is activated. F is reduced to about one-tenth compared to the value without control. Figure 3(b) compares surface pressure distributions of the inviscid flow and surface pressures before and after control is activated. The pressures without control are time-averaged ones, and only the upper surface pressure distributions are presented since the upper and lower pressures are symmetric. The discrepancy between the target inviscid pressure and computed pressure is remarkably reduced, and the computed pressure differs from the target pressure only around the rear part of the cylinder. Since the pressure decreases near the upper and lower parts and increases near the rear

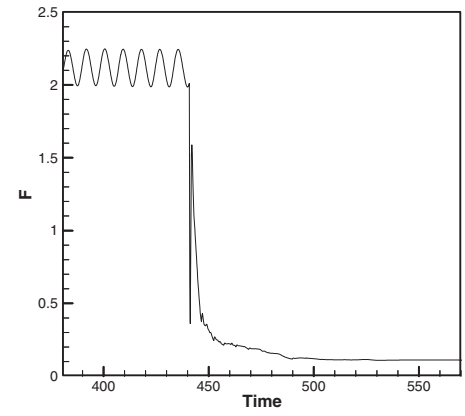

(a) Time history of objective function F.

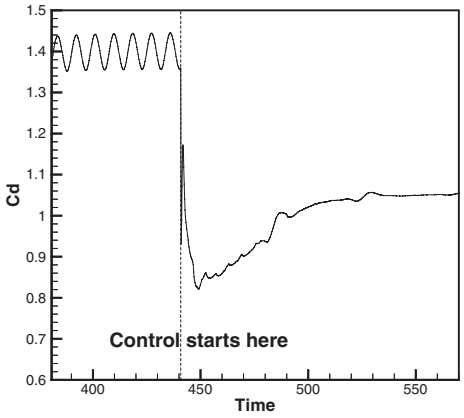

(d) Drag history.

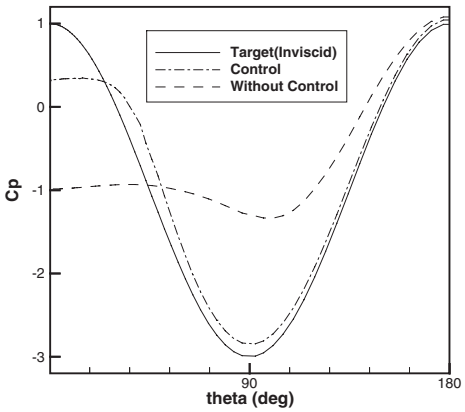

(b) Time-averaged surface pressure distribution.

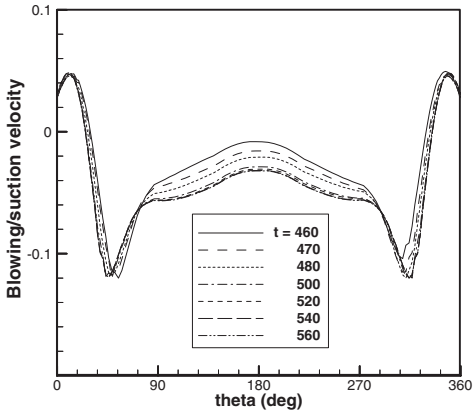

(e) Blowing/suction velocity distributions.

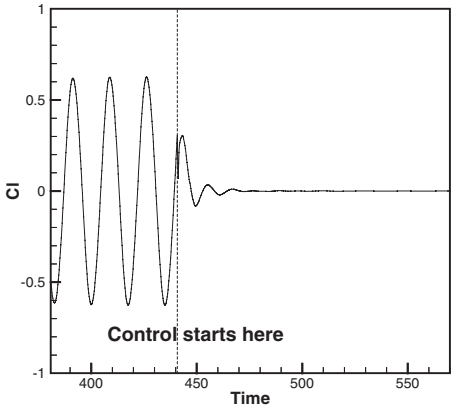

(c) Lift history.

Fig. 3. Vortex shedding control results.

part, the pressure drag would be greatly reduced by the control. As shown in Figs. 3(c) and (d), the fluctuations of the cylinder lift and drag are removed and their magnitudes are remarkably reduced through the control procedure. One can clearly see the effect of the vortex shedding control in Fig. 4, which compares streamlines of the cylinder flow without and with control.

5.3. Airfoil shock buffet control by blowing/suction

In this example and the following one, we deal with a buffet control problem of a supercritical airfoil. Shock buffet[9] is a shock-boundary layer interaction phenomenon causing shock oscillation on the airfoil surface and oscillation of lift and drag, which is a major limiting factor for the cruise speed or lift of transonic transports. The objective of this example is to remove the lift fluctuation of an SC(2)0714 airfoil under buffet flow conditions of $M_\infty = 0.725$, incidence angle of 3.5° and Reynolds number of 15×10^6. Figure 5 shows iso-Mach contours around the airfoil.

The objective function is defined as follows.

$$\text{Minimize} \quad F = |C_l - C_{l0}|, \tag{24}$$

where C_{l0} is the lift coefficient at the time when control is

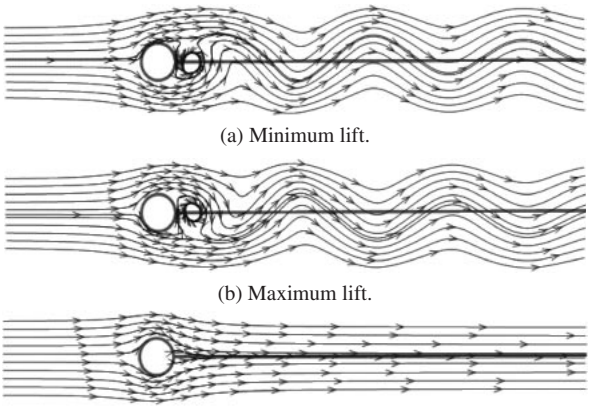

(a) Minimum lift.

(b) Maximum lift.

(c) Wake control result.

Fig. 4. Vortex shedding control results: comparison of streamlines.

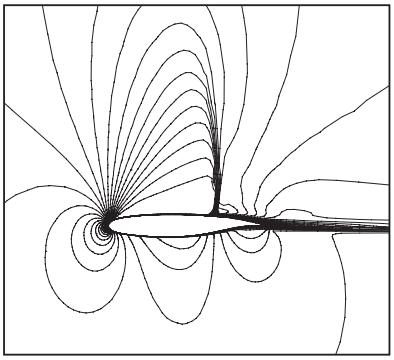

(a) Maximum lift.

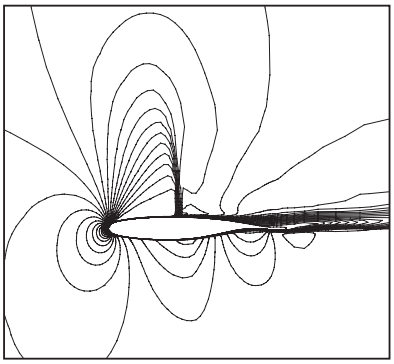

(b) Minimum lift.

Fig. 5. Iso-Mach contours around an SC(2)-0714 airfoil with shock buffeting.

activated. Control parameters are blowing/suction velocities at 12 orifices along the 40–70% chord locations on the upper surface. The adjoint code is used for the computation of sensitivity derivatives.

As shown in Fig. 6(a), the lift of the airfoil is kept almost constant by the control. Figure 6(b) shows the variation of the blowing/suction velocities of the 12 orifices, all of which have the same main frequency. Figure 6(c) shows instantaneous iso-Mach contours around the airfoil under control.

5.4. Airfoil shock buffet control by flap deflection

In this case, the lift oscillation caused by the shock buffet

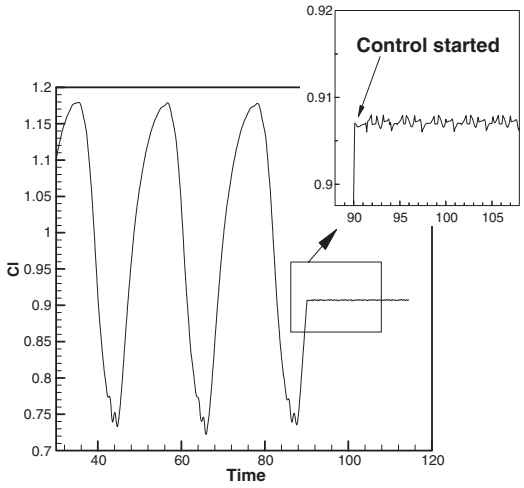

(a) History of lift coefficient.

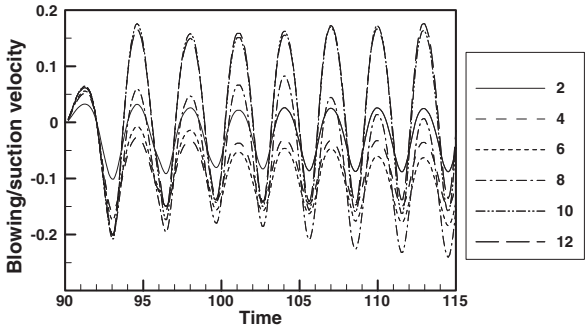

(b) Variation of blowing/suction velocity.

Fig. 6. Shock buffet control results with blowing/suction.

Fig. 7. Plain flap of SC(2)-0714 with 30% chord length.

is removed by adjusting the deflection angle of a plain flap as can be seen in Fig. 7. The clockwise deflection angle is defined to be positive. The same objective function as the previous example is defined as in Eq. (24). We used the direct code for the calculation of sensitivity derivatives since only one control parameter is adopted here.

Figure 8(a) shows the lift history of the airfoil. Unlike the previous control example with blowing/suction, the lift coefficient is kept perfectly constant through control. It is clear from Fig. 8(b) that the unsteady flow has become a steady one by the appropriate deflection of the plain flap. The deflection angle of -3.17° is equivalent to a reduction of the incidence angle by about 1°, and by this effect of incidence angle decrease, the airfoil is now out of the buffet flow condition. Figure 8(c) shows iso-Mach contours of the steady-state flow field obtained through control.

6. Concluding Remarks

We described a robust flow control method using unsteady

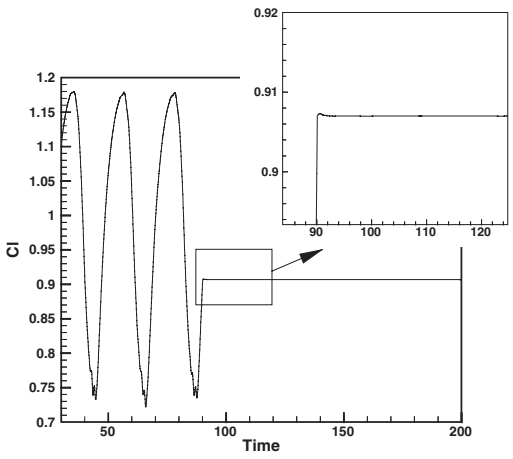

(a) Lift history.

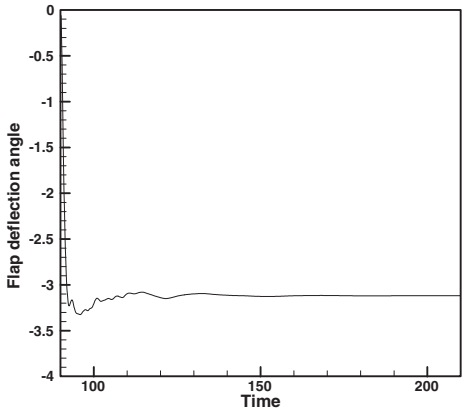

(b) Flap deflection angle variation.

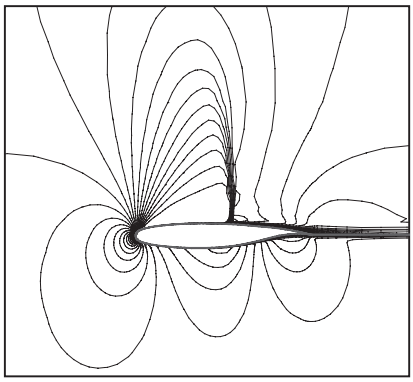

(c) Steady iso-Mach contours around SC(2)-0714 with flap deflection.

Fig. 8. Shock buffet control results with plain flap deflection.

aerodynamic sensitivity analysis via direct differentiation and adjoint methods in a discrete approach. Formulations of the discrete unsteady sensitivity analysis were presented for both sequential and integrated objective functions. The unsteady sensitivity codes were developed from the steady codes and validated for instantaneous objective functions.

With the developed unsteady sensitivity codes, we conducted several suboptimal flow control examples of academic interest using a linear line search method. Flow control examples included circular cylinder lift control, vortex shedding control and transonic airfoil buffet control problems, and gave satisfactory results.

The flow control strategy adopted in this study shows promise for application to various flow control problems since it is robust and problem-independent compared to conventional flow control methods.

References

1) Joslin, R. D., Gunzburger, M. D., Nicolaides, R. A., Erlebacher, G. and Hussaini, M. Y.: A Self-Contained, Automated Methodology for Optimal Flow Control Validated for Transition Delay, NACA CR 198215, ICASE Report No. 95-64, Sep. 1995.
2) Teman, R., Bewley, T. and Moin, P.: Control of Turbulent Flows, Proceedings of the 18th IFIP TC7 Conference on System Modelling and Optimzation, Detroit, MI, July 1997.
3) Min, C. and Choi, H.: Suboptimal Feedback Control of Vortex Shedding at Low Reynolds Numbers, *J. Fluid Mech.*, **401** (1999), pp. 123–156.
4) Mohammadi, B.: Flow Control and Shape Optimization in Aeroelastic Configurations, AIAA 99-0182, Jan. 1999.
5) Kim, H. J., Kim, C., Rho, O. H. and Lee, K.: Aerodynamic Sensitivity Analysis for Navier-Stokes Equations, AIAA 99-0402, Jan. 1999.
6) Hwang, S. W.: Numerical Analysis of Unsteady Supersonic Flow over Double Cavity, Ph.D. Dissertation, Seoul National Univ., Seoul, Korea, 1996.
7) Kim, H. J. and Rho, O. H.: Dual-Point Design of Transonic Airfoils using the Hybrid Inverse Optimization Method, *J. Aircraft*, **34** (1997), pp. 612–618.
8) Nadarajah, S. K. and Jameson, A.: Optimal Control of Unsteady Flows Using a Time Accurate Method, 9th AIAA/ISSMO Symposium on Multidisciplinary Analysis and Optimization Conference, AIAA-2002-5436, September 4–6, 2002, Atlanta, GA.
9) Bartels, R. E.: Flow and Turbulence Modeling and Computation of Shock Buffet Onset for Conventional and Supercritical Airfoils, NASA/TP-1998-206908, Feb. 1998.